Free Radical Biology and Medicine 209 (2023) 116–126

Contents lists available at ScienceDirect

Free Radical Biology and Medicine

journal homepage: www.elsevier.com/locate/freeradbiomed

Photochemically-induced protein tyrosine nitration *in vitro* and *in cellula* by 5-methyl-1,4-dinitro-1*H*-imidazole (DNI): synthesis and biochemical characterization

Natalia Rios [a,b], Adrián Aicardo [a,b,c], Cecilia Chavarría [a,b], Rodrigo Ivagnes [a,b], Mauricio Mastrogiovanni [a,b], Rafael Radi [a,b], José M. Souza [a,b,*]

[a] Departamento de Bioquímica, Facultad de Medicina, Universidad de la República, Av. Gral. Flores 2125, Montevideo 11800, Uruguay
[b] Centro de Investigaciones Biomédicas (CEINBIO), Facultad de Medicina, Universidad de la República, Av. Gral. Flores 2125, Montevideo 11800, Uruguay
[c] Departamento de Nutrición Clínica, Escuela de Nutrición, Universidad de la República, Av. Ricaldoni S/N, Montevideo 11600, Uruguay

ARTICLE INFO

Keywords:
Nitrogen dioxide
Protein nitration
Tyrosine nitration
Photochemical nitration
Free radicals

ABSTRACT

The photochemical nitrating agent 5-methyl-1,4-dinitro-1*H*-imidazole (DNI) has been recently described as an effective tool for nitrating tyrosine residues in proteins under 390 nm irradiation (Long T. et al., 2021). Herein, we describe the one-step synthesis of DNI from the precursor 4-methyl-5-nitro-1*H*-imidazole with good yield (66%) and high purity (>99%). Spectral analysis of DNI reveals two maximum peaks (228 and 290 nm) with maximum nitration yields and kinetics occurring at 290 nm. Electron paramagnetic resonance (EPR)- and mass spectrometry (MS)- spin trapping analysis evidenced the formation of nitrogen dioxide ($^{\bullet}NO_2$) upon irradiation of DNI, implying the homolysis of the N–N bond in the DNI molecule. Irradiation of DNI at 290, 390 nm, or UVA light (315–400 nm), produced tyrosine nitration, with yields approaching *ca.* 30% with respect to DNI at 290 nm exposure. Indeed, using alpha-synuclein as a model protein, the main protein post-translational modification triggered by DNI was the generation of 3-nitrotyrosine as shown by MS analysis. Additionally, the formation of di-tyrosine was also observed. Finally, intracellular $^{\bullet}NO_2$ production upon DNI photolysis in bovine aortic endothelial cells was evidenced by the nitration of the tyrosine analog probe *p*-hydroxyphenylacetic acid (PHPA) and cellular protein tyrosine nitration.

1. Introduction

Protein tyrosine nitration is an oxidative post-translational modification observed *in vivo* caused by a radical-mediated pathway. The replacement of a hydrogen atom in position 3 of the phenol ring of a tyrosine residue by a nitro group (-NO_2), results in the formation of 3-nitrotyrosine (3-NO_2-Tyr) [1]. 3-NO_2-Tyr is considered a biomarker of several pathological conditions [2–7]. Increased levels of 3-NO_2-Tyr and nitrated proteins are found in neurodegenerative diseases [8,9], cardiovascular diseases, inflammation and cancer [10–14]. Also, tyrosine nitration in proteins can induce a loss- or gain-of-function, which could be involved in a pathophysiological cascade [3]. Many oxidants may induce one-electron oxidation in tyrosine residues, such as $^{\bullet}OH$, $^{\bullet}NO_2$, $CO_3^{\bullet-}$, oxo-metal compounds ($O{=}Mn^{IV}$), and compounds I and II of peroxidases (*e.g.* myeloperoxidase) to tyrosyl radical; the latter can combine with $^{\bullet}NO_2$ to yield 3-NO_2-Tyr [1]. Peroxynitrite ($ONOO^-$/ONOOH) is one of the main nitrating agents in biological systems since it can undergo homolysis to $^{\bullet}OH$ and $^{\bullet}NO_2$ [15–19].

Tetranitromethane (TNM) is a well-established chemical nitrating agent commonly employed to generate 3-NO_2-Tyr residues in proteins. Indeed, TNM reacts with the phenoxide anion *via* a free-radical pathway with the formation of $^{\bullet}NO_2$ and tyrosyl radical intermediates [20]. TNM,

Abbreviations: $ABTS^{2-}$, 2,2′-azino-bis(3-ethylbenzothiazoline-6-sulfonate); BAECs, bovine aortic endothelial cells; DNI, (5-methyl-1,4-dinitro-1*H*-imidazole); DMPO, 5,5-dimethyl-1-pyrrolin; DTPA, diethylenetriaminepentaacetic acid; EtOAc, ethyl acetate; EPR, electronic paramagnetic resonance; NO_2-HPA, 4-hydroxy-3-nitrophenylacetic acid; NI, 4-methyl-5-nitro-1*H*-imidazole; 3-NO_2-Tyr, 3-nitrotyrosine; NMR, nuclear magnetic resonance; MS, mass spectrometry; PBS, phosphate-buffered saline; PHPA, *p*-hydroxyphenylacetic acid; PMSF, phenylmethylsulphonyl fluoride; α-syn, alpha-synuclein; TNM, tetranitromethane; TLC, thin layer chromatography.

* Corresponding author. Departamento de Bioquímica, Facultad de Medicina, Universidad de la República, Av. Gral. Flores 2125, Montevideo 11800, Uruguay.
E-mail address: jsouza@fmed.edu.uy (J.M. Souza).

https://doi.org/10.1016/j.freeradbiomed.2023.09.038
Received 24 August 2023; Received in revised form 21 September 2023; Accepted 29 September 2023
Available online 30 September 2023

used at pH 8, shows mild selectivity toward tyrosine residues, but it may also induce the nitration of tryptophan, as well as the oxidation of cysteine, methionine and histidine [21]. Additionally, nitrite (NO_2^-) at acidic pH is capable of nitrating tyrosine residues in proteins [22]. An alternative nitration approach involves employing an electrophilic aromatic substitution with nitronium ion (NO_2^+) as the electrophile, derived from the inorganic salt nitronium borofluorate (NO_2BF_4) [23]. This method exhibits the capacity to promote the nitration of free Tyr [24], as well as Tyr residues in protein, along with the detection of other modifications like carbonylation [25].

Recently, DNI (5-methyl-1,4-dinitro-1*H*-imidazole) was described as a photochemical nitrating agent able to nitrate tyrosine residues when irradiated at 390 nm, and also able to oxidize cysteine residues to disulfides [26]. The properties of organic nitramines (RN-NO_2), as photochemical $^{\bullet}NO_2$ donors, are well known in the field of material science [27,28]. Aliphatic and monocyclic nitramines like cyclitrimethylenetrinitramine (RDX) and cyclotetramethylenetetranitramine (HMX), or polycyclic nitramine hexanitrohexaazaisowurtzitane (HNIW) supporting 3, 4 or 6 N–NO_2 groups respectively, are energetic materials with highly exergonic reactions [29,30]. These chemical compounds are commonly used in explosives and propellants. It is suggested that these characteristics are related to their ability to produce $^{\bullet}NO_2$ during thermolysis or photolysis, with little biochemical and biological applications [28–30]. DNI is a mono-nitramine, with only one N–NO_2 group, supported on an imidazole ring (Scheme I). This structural configuration makes it a more suitable reagent for applications in the biochemistry field compared to aliphatic multiple-nitramines.

Given that the original article [26] did not contain a description of how DNI was obtained or synthesized, we were motivated to develop a preparation method, and then conducted an expanded biochemical characterization exploring its cellular application. In this manuscript, we describe the synthesis of DNI, its photochemical properties with different irradiation sources, the reaction mechanism of as a nitrating agent, and its capacity to promote protein tyrosine nitration *in vitro* and *in cellula*. Our results further characterize and support DNI as a suitable photochemical agent for generating 3-NO_2-Tyr in isolated proteins and cells.

2. Materials and methods

2.1. Reagents

4-methyl-5-nitro-1*H*-imidazole was purchased from Aaron Chemicals LLC (NI). Tyrosine (Tyr), 3-nitrotyrosine (3-NO_2-Tyr), *p*-hydroxyphenylacetic acid (PHPA), 4-hydroxy-3-nitrophenylacetic acid (NO_2-HPA) 2,2′-azino-bis(3-ethylbenzothiazoline-6-sulfonic acid) diammonium salt (ABTS), diethylenetriaminepentaacetic acid (DTPA), sodium nitrite ($NaNO_2$), and all other reagents were purchased from Sigma-Aldrich. 5,5-dimethyl-1-pyrroline *N*-oxide (DMPO) from Enzo Life Science. [$^{13}C_9$,^{15}N]-tyrosine and 3-nitro[$^{13}C_6$]-tyrosine stable labelled internal standards were purchased from Cambridge Label Isotopes Inc. Peroxynitrite was synthesized from sodium nitrite and H_2O_2 under acidic conditions in a quenched-flow reactor as described previously and stored at −80 °C [31]. Peroxynitrite concentrations were determined spectrophotometrically at λ=302 nm (ε=1670 $M^{-1}cm^{-1}$), and nitrite contamination was typically less than 20% with respect to peroxynitrite [31]. All assays were performed in phosphate buffer (100 mM, pH 7.4 or pH 6.0) containing diethylenetriaminepentaacetic acid (DTPA, 0.1 mM) to eliminate potential metal trace interference.

2.2. Synthesis of 5-methyl-1,4-dinitro-1H-imidazole (DNI)

DNI was obtained in one-step reaction through a general method for *N*-nitroimidazoles preparation [32]. A suspension of 4-methyl-5-nitro-1*H*-imidazole (250 mg, 1.96 mmol) in glacial acetic acid (9.0 mL) was added to a round bottom flask and treated dropwise with concentrated nitric acid (2.2 mL). To the solution was added, with cooling, acetic anhydride (6.0 mL) and the reaction mixture was stirred for 1 h at room temperature. Monitoring by TLC (*n*-hexane/EtOAc (1:1)) showed a complete conversion and only a single product was present. After pouring onto ice the mixture was extracted with dichloromethane (5 x 10 mL), the extracts were washed with aqueous sodium bicarbonate (2 x 15 mL), and dried over anhydrous Na_2SO_4. After removal of solvent, 5-methyl-1,4-dinitro-1*H*-imidazole was obtained as a highly pure white solid. Yield = 66% (221 mg). Purity (>99%).

^{1}H RMN (400 MHz, $(CD_3)_2CO$) δ 2.99(3H s), 8.70 (1H, s).
^{13}C NMR δ: 10.7, 128.3, 131.1
MS (EI): *m/z* (%) = 172 (23.5), 126 (2.0), 46 (100).

Analytical TLC was performed on silica gel TLC-PET foils (Fluka). Plates were visualized with UV light (λ=254 nm). ^{1}H NMR and ^{13}C NMR spectra were recorded on a Bruker DPX-400 instrument, with $(CD_3)_2CO$ as the solvent. The chemical shifts values are expressed in parts per million relative to tetramethylsilane as internal reference. Mass spectra were recorded on a Shimadzu GC/MS QP 1100 EX mass spectrometer operating at an ionization potential of 70 eV by direct sample injection (DI).

2.3. UV–Vis absorption spectra

Electronic absorption spectra were recorder on a Shimadzu UV-2450 UV–Vis spectrophotometer in H_2O or phosphate buffer (50 mM, pH 7.4 containing 0.1 mM DTPA).

2.4. Lamp sources

For monochromatic light irradiation (228 nm, 290 nm or 390 nm) a JASCO 8500 Spectrofluorometer was used. Also, UV–Vis lamp OSRAM Ultra Vitalux 300 W 230 V E27, radiated power 315–400 nm (UVA) 13.6 W, and 280–315 nm (UVB) 3.0 W, dimensions diameter 127.0 mm x length 185.0 mm, were used.

For cellular assays light irradiation was performed using an UVA (315–400 nm) lamp PHILIPS Actinic BL 8W/10 1FM 10X25CC, dimensions diameter 16 mm x length 288.3 mm.

2.5. HPLC analysis

Analysis, separation and quantification of 3-NO_2-Tyr, di-Tyr, DNI and NI were performed by HPLC (Agilent Technologies 1200) coupled to UV–visible and fluorescence detectors. The reactants and products of the reaction of DNI with tyrosine were separated using a column TSKgel ODS 120 Å, 4.6 x 25 cm 5 μm (Tosho Bioscience, catalogue number 07124). The mobile phases were A: 50 mM formic acid pH 3, and B: methanol with 50 mM formic acid pH 3. The HPLC chromatography was performed at a 1 mL/min flow, with 3% B mobile phase during 5 min, a linear gradient to 20% B mobile phase in 30 min, and an equilibration from 31 to 40 min with 3% mobile phase B. The chromatography was followed at 280 and 360 nm in the UV–visible detector and the fluorescence detection was fix at λ=294 nm for excitation and λ=410 nm for the emission. All peaks were assigned using the corresponding standards. 3,3′-dityrosine was synthesized as reported previously [33].

2.6. ABTS assay

A mixture of 2,2′-azino-bis(3-ethylbenzothiazoline-6-sulfonic acid) diammonium salt (ABTS) (1 mM) and DNI (0.1 mM) in phosphate buffer (50 mM, pH 7.4 containing 0.1 mM DTPA), was irradiated under 290 nm using a JASCO 8500 Spectrofluorometer with magnetic stirring at room temperature. The formation of $ABTS^{\bullet-}$ was spectrophotometrically monitored every 15 min for 90 min on a Shimadzu UV-2450 UV–Vis spectrophotometer. $\varepsilon_{728\ nm}$ = 1.5 x 10^4 $M^{-1}cm^{-1}$ [34].

2.7. EPR experiments

EPR experiments were recorded on a MiniScope MS 400 Magnettech by Freiberg Instruments. EPR measurements were taken at room temperature with sweep-time 60 s, modulation amplitude 1 G, MW-Att. 10.0000 dB. Solvents used include CH_3CN, H_2O or a potassium phosphate buffer (50 mM, pH 7.4, containing 0.1 mM DTPA).

The samples were introduced in a quartz flat cell and irradiated in the EPR cavity with a UV–Vis lamp OSRAM Ultra Vitalux 300 W 230 V E27, radiated power 315–400 nm (UVA) 13.6 W and 280–315 nm (UVB) 3.0 W, dimensions diameter 127.0 mm x length 185.0 mm. The spectrum simulation was carried out by an automatic fitting program [35].

Alternatively, $^{\bullet}NO_2$ was generated by UV photolysis of nitrite as follows: a solution containing DMPO (45 mM) and $NaNO_2$ (300 mM) in PBS pH 7.4 containing 0.1 mM DTPA was transferred to a quartz flat cell and irradiated in the EPR cavity with a UV–Vis lamp OSRAM Ultra Vitalux 300 W 230 V E27, radiated power 315–400 nm (UVA) 13.6 W and 280–315 nm (UVB) 3.0 W, dimensions diameter 127.0 mm x length 185.0 mm. The procedure was repeated for DMPO (45 mM) alone in PBS (50 mM pH 7.4 containing 0.1 mM DTPA), and DNI (45 mM) in absence of DMPO in PBS (50 mM pH 7.4 containing 0.1 mM DTPA).

2.8. Detection of DMPO adducts by MS

A mixture of DNI (45 μM) and DMPO (45 μM) in H_2O was irradiated by a UV–Vis lamp OSRAM Ultra Vitalux 300 W 230 V E27, radiated power 315–400 nm (UVA) 13.6 W and 280–315 nm (UVB) 3.0 W, dimensions diameter 127.0 mm x length 185.0 mm, and the solution analyzed by tandem mass spectrometry (MS/MS) by direct injection. Mass spectrometry analysis were performed on a hybrid triple quadrupole –linear ion trap equipment (QTRAP4500, ABSciex) by direct infusion at 5 μL/min employing an electrospray ionization source (ESI). Mass spectrometer was set on negative Precursor Ion mode. The ion of *m/z* 114 was chosen as a reporter ion of DMPO adduct, and scan was performed from *m/z* 50 to *m/z* 250. Electrospray voltage, declustering potential and collision energy were set at 5.5 kV, 30 V and 30, respectively. Acquisition was performed employing Analyst 1.6.2, and visualization and data analysis were performed employing PeakView 2.1 (ABSciex). The procedure was repeated for DMPO (45 μM) in H_2O alone and DNI (45 μM) in H_2O in absence of DMPO.

2.9. α-Synuclein purification

Human recombinant α-syn was purified from E. *coli* BL21. Expression was induced adding IPTG 0.5 mM into LB growth medium at exponential growth face. The expressed protein was purified as described in Ref. [36]. Briefly, bacterial pellets were resuspended in 10 mM Tris, 750 mM NaCl, 1 mM PMSF and 1 mM EDTA pH 7.5 buffer and sonicated during 10 s eight times. The cell suspension was boiled and centrifuged at 10000 rpm for 15 min at 4 °C and the supernatant was incubated with streptomycin sulphate (10 mg/mL) and ammonium sulphate (0.36 g/mL), centrifugated and dialyzed against 10 mM Tris buffer 1 mM EDTA pH 7.5. The dialyzed sample was loaded into a resource Q ionic exchange column, and α-syn was purified by HPLC using a NaCl gradient 0–1 M. The fraction obtained was dialyzed against a 5 mM Tris, 1 mM EDTA, pH 7.5. The purification was confirmed using 12% SDS–PAGE, and the pure protein was diluted in 10 mM HEPES (pH 7.4) and stored at −80 °C.

2.10. Western-blot

Recombinant α-syn (50 μM) was exposed to DNI (250 μM), loaded on 12% PAGE and electrophoresis was carried out with Tris-SDS running buffer. Proteins were transferred on 0.2 μm nitrocellulose membranes and incubated for 1 h in blocking solution (5% Bovine Serum Albumin solution in PBS). Blocked membranes were incubated overnight at 4 °C with anti 3-nitrotyrosine monoclonal antibody (HM11 Invitrogen) [37], and also anti α-syn monoclonal antibody (BD transduction laboratories). Then, membranes were incubated for 1 h at room temperature with anti-mouse (IRDye 680RD LI-COR) as secondary antibody. Images were taken with Odyssey Fc (LI-COR Biotechnology, Lincoln, NE) imaging system. Membranes were washed with 0.1% PBS-tween three times between each incubation step.

2.11. Cell culture

Primary bovine aortic endothelial cells (BAECs) were obtained from Genlantis. Cultures of BAECs cells were maintained in DMEM (Sigma D5523) supplemented with penicillin (100 units mL^{-1}), streptomycin (100 μg mL^{-1}) and FBS (10% v/v) at 37 °C in a humidified atmosphere (5% CO_2).

2.12. Cytotoxicity assay

For DNI cytotoxicity assay, confluent BAECs were incubated with DNI (0–1000 μM) in Dulbecco's phosphate buffered saline solution (dPBS) consisting in NaCl (137 mM), Na_2HPO_4 (8.1 mM), $CaCl_2$ (0.9 mM), $MgCl_2$ (0.5 mM), KCl (2.7 mM) and KH_2PO_4 (1.45 mM), pH 7.4, and exposed to UVA light for 10 min. Then, cells were washed with dPBS to remove photolysis products and remnant not decomposed DNI. Subsequently, fresh culture media was added and cell were cultured for 24 h before viability was measured. Cell viability was measured by reduction of tetrazolium salt MTT (3-(3,4-dimethylthiazol-2-yl)-2,5-bromide diphenyltetrazolium) to a blue formazan product due to the activity of flavin-dependent dehydrogenases by measuring the absorbance at 570 nm (Varioskan Flash) [38].

2.13. Intracellular PHPA nitration

Confluent BAECs were incubated with PHPA (1 mM) in dPBS, for 30 min at 37 °C in a humidified atmosphere (5% CO_2), washed in order to eliminate the non-incorporated probe, added new dPBS and then DNI (250 μM) was incorporated. After that, cells were exposed to UVA light for 10 min, washed once with dPBS and cellular content was extracted with acetonitrile, dry in SpeedVac Concentrator (Thermo Scientific, Savant SPD1010) and analyzed by HPLC-MS.

NO_2-HPA detection and quantitation was performed by HPLC-MS/MS analysis. Liquid chromatography was performed on a reversed phase column, Prodigy ODS(2) 5μ, 150 x 2.0 mm (Phenomenex) employing a linear gradient of acetonitrile containing 0.1% formic acid (B) in nanopure water containing 0.1% formic acid (A) as follows: 25% B from 0 to 8 min, 25%–90% B from 8 to 10 min, maintain at 90% B for 4 min and re-equilibrate at 25% B for 10 min, at a flow rate of 200 μL/min. Mass spectrometer (QTRAP4500, ABSciex) was set in negative MRM mode, electrospray voltage and declustering potential were set to −4.5 kV and −30 V, respectively, and the monitored transitions were 151.1/107.0 and 151.1/79/0 for PHPA and 195.9/122.0; 195.9/46.0; 195.9/152.0 for NO_2-HPA, with optimized collision energies for each transition. Quantitation was performed against an external calibration curve employing the most sensitive transition. In addition, an internal calibration curve for NO_2-HPA quantification was performed. For these purposes, BAECs were pre-incubated with NO_2-HPA standard (0, 50, 100, 250, 500, 1000 nM) in dPBS, washed, and the cellular content extracted with acetonitrile, dry and analyzed as before. Also, NO_2-HPA was quantified in the extracellular media of the standard curve and 38% of the total NO_2-HPA in the cell extracts was estimated. PHPA external calibration curve was prepared in cell lysate solution in order to compensate potential matrix interferences in the whole processing and analysis.

2.14. DNI and UVA light induced intracellular protein tyrosine nitration

In order to evidence protein tyrosine nitration in cells, we analyzed the protein fraction obtained from cells loaded with DNI and exposed to UVA light. Briefly, confluent BAECs cultures were washed with dPBS to remove culture media, then new dPBS with or without DNI (250 μM) was added. After that, cells were exposed to UVA light for 10 min, dPBS was removed, cells were trypsinized, resuspended and centrifuged at 1500G for 5 min. Then, cell lysis was performed by adding 1:20 diluted PBS (containing protease inhibitor mix (SIGMAFAST™ Protease Inhibitor Cocktail) to the cell pellet and sonication for 20 min. Total protein content was measured by BCA assay and lysates were stored at −20 °C until analysis.

Sample processing was performed as in Ref. [39] and quantitation of 3-nitrotyrosine was performed as in Ref. [40] with minor modifications. Cell lysates samples containing ~80 μg protein were submitted to protein precipitation with trichloroacetic acid 8% v/v and centrifugation at 14000*g*, 4 °C, 30 min. Pellets were spiked with stable labelled internal standards; [$^{13}C_9$,^{15}N]-tyrosine (2500 pmol) and 3-nitro[$^{13}C_6$]-tyrosine (100 pmol), and submitted to hydrolysis in methanesulfonic acid with 0.2% w/v tryptamine at 110 °C, overnight. Amino acids were partially purified by solid-phase extraction using Strata SCX tubes (55 μm, 70 Å, 100 mg/1 mL) and analyzed by LC-MS/MS.

Tyrosine and 3-nitrotyrosine were quantified by LC-MS/MS in positive ion mode using a QTRAP 4500 mass spectrometer. Samples were separated by gradient elution using a reversed phase column (Zorbax Eclipse XDB C18, 5 μm, 150 x 2.0 mm, Agilent) with formic acid 0.1% w/w in nanopure H_2O (Solvent A) and formic acid 0.1% w/w in water (Solvent B). Elution gradient was from 5% B to 40% B over 15 min at 500 μL/min, 30 °C. Ion source and gasses parameters were set as follows: IS: 5500 V; TEM: 600 °C; GS1: 30; GS2: 30; CUR: 50. Analyzer was set in positive MRM mode including two transitions per analyte; 3-NO_2[$^{12}C_6$]Tyr (*m/z* 227/181, and 210); 3-NO_2[$^{13}C_6$]Tyr (*m/z* 233/187, and 216); [$^{12}C_6$]Tyr (*m/z* 182/136, and 165); and [$^{13}C_9$,$^{15}N_1$]Tyr (*m/z* 192/145, and 174). Tyrosine oxidation during sample processing was minimized performing acid hydrolysis with the addition of tryptamine and under vacuum to prevent O_2-dependent processes. Nonetheless, artefactual nitration was analyzed also monitoring the nitrated tyrosine internal standard, that is; 3-NO_2[$^{13}C_9$,$^{15}N_1$]Tyr (*m/z* 237/190, and 219) [40]. Tyrosine and 3-nitrotyrosine content in samples were calculated according to area ratio to the corresponding internal standard and corrected after adjusting for the level of artefactual generation (which was controlled to be <10%).

3. Results and discussion

3.1. Synthesis and characterization of 5-methyl-1,4-dinitro-1H-imidazole

A general method for *N*-nitroimidazoles preparation was carried out to obtain DNI in one-step [32]. 4-methyl-5-nitro-1*H*-imidazole treated with excess of nitric acid in acetic anhydride/acetic acid gave 5-methyl-1,4-dinitro-1*H*-imidazole in good yield (66%), Scheme 1. The nitration reaction is regioselective on the annular nitrogen atom more remote from the nitro substituent (N2), probably governed by a combination of steric and electronic effects of the substituents, giving DNI[1] [41] as a single product with high purity (>99%), (Supplementary information, Fig. S1).

The UV–Vis absorption spectra of DNI shows a maximum peak in the region between 220 and 240 nm (λ_{max} = 228 nm) corresponding to the nitramine group (RN-NO_2) [42], and a second broad peak in the

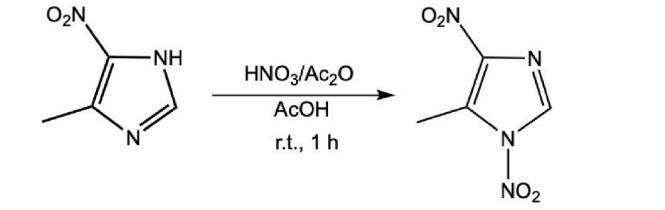

4-methyl-5-nitro-1*H*-imidazole 5-methyl-1,4-dinitro-1*H*-imidazole **(DNI)**

Scheme 1. Synthesis of DNI. DNI was obtained in a one-step *N*-nitration reaction from 4-methyl-5-nitro-1*H*-imidazole as a single product in good yield (66%) and high purity (>99%).

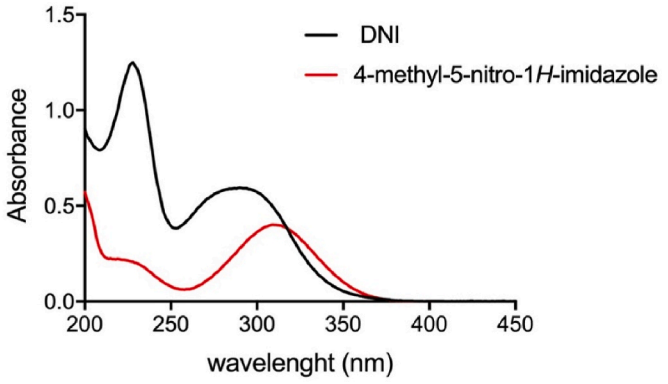

Fig. 1. UV–Vis absorption spectra of DNI (0.1 mM) or 4-methyl-5-nitro-1*H*-imidazole (0.1 mM) in H_2O.

260–330 nm region (λ_{max} = 290 nm, $\varepsilon = (5800 \pm 150)\ M^{-1}cm^{-1}$), Fig. 1. Previously report by Long et al. [26], studied nitration of phenol derivatives, and tyrosine residus in proteins by DNI under 390 nm irradiation. Since at 390 nm DNI has marginal absorption intensity, we also decided to study the photolytic reaction at 228 nm and 290 nm.

3.2. Nitration reaction at different wavelengths

First, using the amino acid tyrosine (Tyr) as a molecular target for nitration, we evaluated how irradiation of DNI under different wavelengths (228 nm, 290 nm or 390 nm) by a monochromatic light source, can modulate nitration reaction yield and kinetics.

In different experiments, Tyrosine (0.5 mM) was irradiated at 228 nm, 290 nm or 390 nm in presence of DNI (0.5 mM) in PBS at pH 6.0 or pH 7.4, and the products analyzed by HPLC, shown in Figs. 2 and 3. No 3-NO_2-Tyr formation was observed under irradiation at 228 nm, while a rapid 3-NO_2-Tyr formation was observed when the mixture was exposed to 290 nm over time, concomitant with a rapid DNI consumption and formation of the sub-product 4-methyl-5-nitro-1*H*-imidazole (nitroimidazole, NI), Fig. 3. In these conditions a minor fraction of di-Tyr was formed (<2%) as evidenced by HPLC with fluorescence detection (Fig. 2). Irradiation of DNI under 390 nm was evaluated as well, and slow kinetics of nitration reaction was observed, Fig. 3.

Similar behavior was noted in both pH, 6.0 and 7.4, however a lower offset (final concentration) for 3-NO_2-Tyr formation at pH 7.4 was observed, as discussed below, (Fig. 3 and Table S1).

3.3. Nitration reaction yield

p-Hydroxyphenylacetic acid (PHPA), a Tyr soluble analogue, was used as a probe to evaluate its nitration to NO_2-HPA by DNI photolysis under different light sources (monochromatic 290 nm or 390 nm; or

[1] The incorporation of the nitro group on the N atom gives this locant the highest priority according to the IUPAC nomenclature system, therefore, DNI is named as 5-methyl-1,4-dinitro-1*H*-imidazole. [41] McNaught, A.D. and A. Wilkinson, *Compendium of chemical terminology. IUPAC recommendations*. Vol 1669, Oxford: Blackwell Science, 1997.

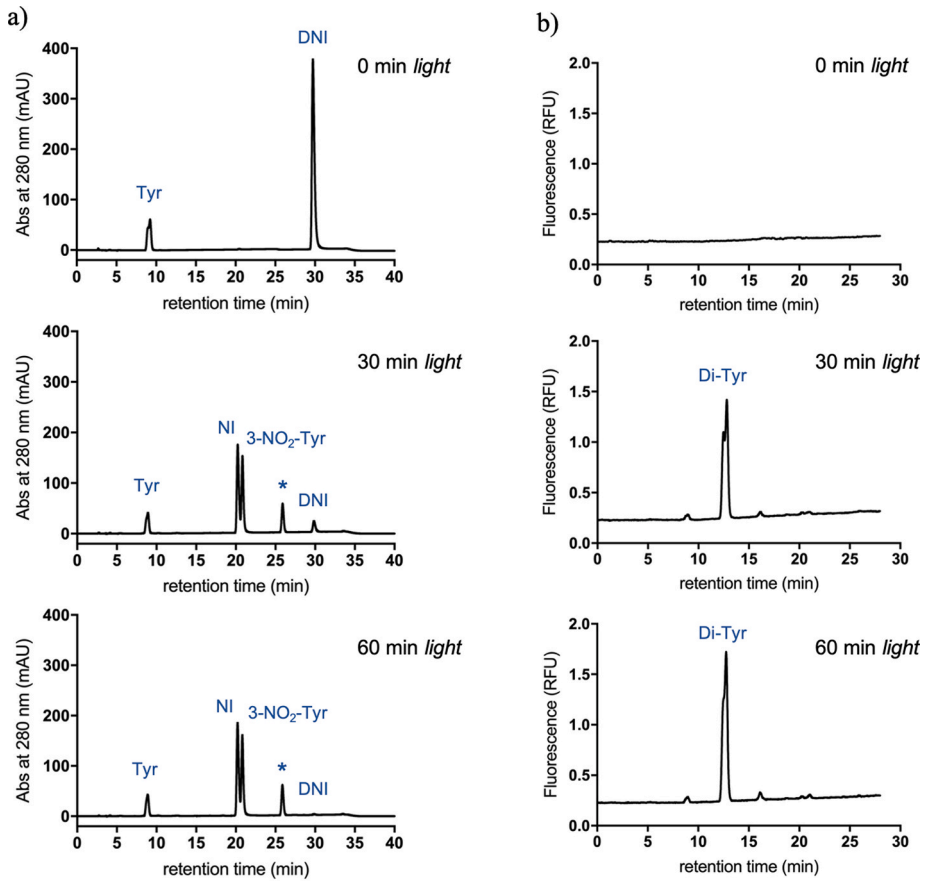

Fig. 2. ***In vitro*** **DNI-mediated free tyrosine nitration.** a) HPLC chromatograms (detected at $\lambda_{Abs} = 280$ nm) after 0, 30, or 60 min irradiation at 290 nm of mixtures containing DNI (0.5 mM) and Tyr (0.5 mM) in phosphate buffer (100 mM, pH 6.0). All peaks were assigned comparing the retention time with standards, except for (*) peak which corresponds to 2,4-dinitroimidazole as reported previously [26]. b) Same as a) but showing fluorescence detection peaks ($\lambda_{exc} = 294$ nm, $\lambda_{em} = 410$ nm). 3,3′-dityrosine (Di-Tyr) peak was assigned using a standard. No additional peaks were observed over 30 min with fluorescence detector.

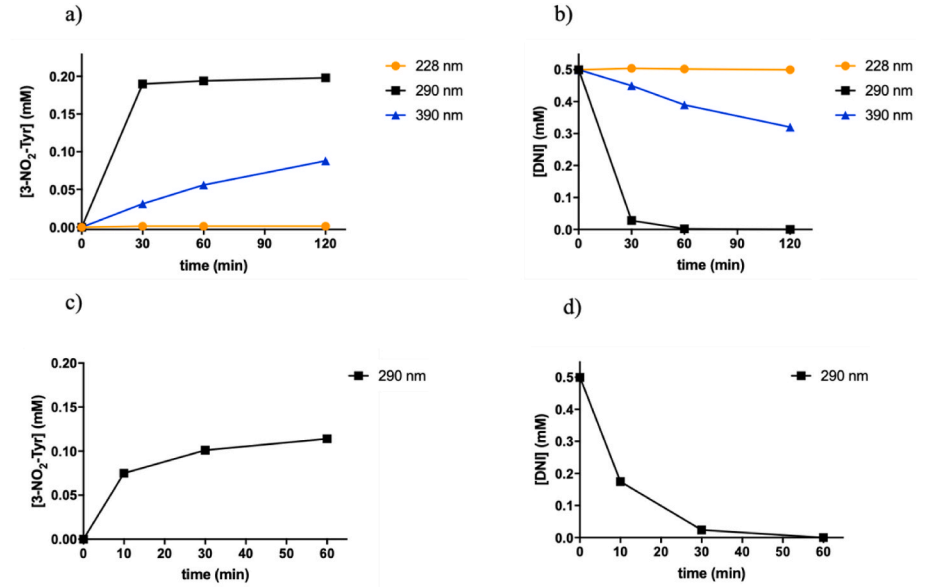

Fig. 3. 3-NO_2-Tyr formation and DNI consumption at different pH**.** A mixture containing Tyr (0.5 mM) and DNI (0.5 mM) in phosphate buffer (100 mM) was irradiated under different wavelengths, at pH 6, panel a) and b); or pH 7.4, panel c) and d). 3-NO_2-Tyr concentrations were calculated using the peak area of 3-NO_2-Tyr standard in the chromatographic analysis.

Table 1
Comparison of nitration reaction yields (%) at different pH under 290 nm monochromatic irradiation or UVA light.

Target	pH	**Nitration yield at 290 nm** (%)	**Nitration yield at UVA** (%)
PHPA	6.0	(32.6 ± 0.8)	*n.d.*
PHPA	7.4	(26.4 ± 6.2)	(19.6 ± 2.0)
Tyr	7.4	(9.6 ± 0.2)	(9.7 ± 0.1)

Nitration reaction yields were determined as [NO_2-HPA]/[DNI] (%) or [3-NO_2-Tyr]/[DNI] (%) for PHPA or Tyr respectively; *n.d.* stands for not determined.

UVA light (315–400 nm)). Excess of target (1 mM and 2 mM PHPA) in the presence of DNI (0.25 mM) in PBS 100 mM at pH 6.0 and pH 7.4 was irradiated under 290 nm or 390 nm for 30 min, and the content analyzed by HPLC, Supplementary information, Fig. S2, panel a). A nitration yield of 32% based on initial DNI concentration was determined at pH 6.0, and 26% nitration yield at pH 7.4 (corresponding 83 μM and 65 μM NO_2-HPA respectively) upon a 30 min 290 nm monochromatic irradiation, Table 1. Under these conditions DNI was practically consumed (1.5 μM remnant DNI) as shown in Supplementary information, Fig. S2, panel a).

However, a 30 min irradiation at the higher wavelength of 390 nm resulted on a lower NO_2-HPA formation at pH 6 or pH 7.4 (30 μM and 17 μM NO_2-HPA respectively), since most DNI was unreacted.

The yields of NO_2-HPA formation are in agreement with the levels of 3-NO_2-Tyr obtained shown in Fig. 3, where a slow nitration kinetic was observed upon 390 nm irradiation with respect to a 290 nm irradiation, Fig. 3. Furthermore, DNI-mediated nitration of PHPA under UVA light gave a 19.6% nitration yield at pH 7.4 (44 μM NO_2-HPA), calculated at 60 min irradiation time when DNI was fully consumed, Fig. S2, panel b), Table 1.

Additionally, nitration yield was determined with Tyr (0.5 mM) and DNI (0.125 mM) in PBS 100 mM at pH 7.4, under 290 nm and UVA light irradiation, Table 1. A nitration yield of *ca.* 10% was obtained in both conditions.

Previously, Beckman et al. reported a ~7% nitration yield of PHPA by peroxynitrite (potassium phosphate buffer 50 mM containing 0.1 mM DTPA at pH 7.4 at 37 °C) [43].

Results from our group showed a nitration yield of Tyr of ~9–10% or ~5% by bolus addition or a flux of peroxynitrite, respectively, at pH 7.4 [44]. Additionally, nitration yields with peroxynitrite using a hydrophobic analogue of Tyr, BTBE (*N-t*-BOC L-tyrosine *tert*-butyl ester) incorporated to 1,2-dilauroyl-*sn*-glycero-3-phosphocholine liposomes were ~2.5% [45]. Nitration yields in the presence of DNI at pH 7.4 for Tyr were similar to those with peroxynitrite and higher for PHPA at both pH (Table 1). The dissimilar nitration yields as a function of the tyrosine analog and pH could be attributed to differential tendencies for dimerization [46,47].

These experiments demonstrate also the significance of the light source, as it can impact both the yields and kinetics of the nitration reaction.

3.4. Study of the reaction mechanism

Photolytic degradation of monocyclic nitramines RDX and HMX, or polycyclic nitramine HNIW produces $^{\bullet}NO_2$ by a radical mechanism as previously reported [29,30]. In this way, Long et al. suggested a radical mechanism of DNI photolytic nitration since radical trapping reagents (*e.g.* BHT, TEMPO, and 1,1-diphenylethylene) decreased the nitration yields of phenol derivatives [26]. Hence, the homolytic scission of the N–NO_2 bond of DNI, and the concomitant $^{\bullet}NO_2$ production was analyzed by $ABTS^{2-}$ scavenging assay, EPR experiments and tandem mass spectrometry (MS/MS) analysis to evidence radical formation ($^{\bullet}NO_2$ or nitroimidazole radical, $NI^{\bullet}$). Finally, we studied if O_2 has any contribution on the reaction mechanism of tyrosine nitration.

Since $^{\bullet}NO_2$ does not absorb strongly, the formation of the intense chromophore $ABTS^{\bullet-}$as a reporter molecule was employed[2] [48]. Oxidation of 2,2′-azino-bis(3-ethylbenzothiazoline-6-sulfonic acid ($ABTS^{2-}$) by $^{\bullet}NO_2$ radical yields the oxidized form $ABTS^{\bullet-}$ (equation (1)), with a fast second-order rate constant of $k = 2.2\ x10^7\ M^{-1}s^{-1}$ [34]. $ABTS^{\bullet-}$ has a green-blue color, which absorbs strongly in the visible region, with an extinction coefficient of $1.5\ x\ 10^4\ M^{-1}cm^{-1}$ at 728 nm. DNI (0.1 mM) was irradiated under 290 nm in presence of $ABTS^{2-}$ (1 mM) in PBS 50 mM (pH 7.4, containing 0.1 mM DTPA), and the reaction was spectrophotometrically monitored, Fig. S3.

$$ABTS^{2-} + {}^{\bullet}NO_2 \rightarrow ABTS^{\bullet-} + NO_2^{-}\ k = 2.2\ x10^7\ M^{-1}s^{-1} \quad (1)$$

An $ABTS^{\bullet-}$ formation rate of 0.2 μM/min (over 60 min) was observed. Although, the reaction of $^{\bullet}NO_2$ with $ABTS^{2-}$ is extremely fast ($k = 2.2\ x10^7\ M^{-1}s^{-1}$) [34], the rate of $ABTS^{2-}$ oxidation obtained by DNI-mediated oxidation could have other contributions due to $NI^{\bullet}$. Additional future experiments are needed to determine the reaction rate of $NI^{\bullet}$ with $ABTS^{2-}$.

The higher $ABTS^{\bullet-}$ concentration obtained (~10 μM), was lower than expected based on the nitration yield (Table 1), probably due to secondary radical reactions that compete with either $ABTS^{2-}$, $ABTS^{\bullet-}$, $^{\bullet}NO_2$ or $NI^{\bullet}$ [49]. Nevertheless, the time course of $ABTS^{\bullet-}$ formation (Fig. S3) is in good agreement with a complete DNI consumption after 60 min irradiation determined in previous results, Fig. 3.

Furthermore, EPR experiments were carried out in order to evidence $^{\bullet}NO_2$ or $NI^{\bullet}$ formation due to DNI photolysis. DMPO was used as the spin-trapping agent. A solution containing DMPO (45 mM) and DNI (45 mM) in PBS (pH 7.4 containing 0.1 mM DTPA) was added to an EPR flat cell and irradiated with UV–Vis lamp in the EPR cavity for 3, 8 and 10 min, Fig. 4. The different irradiation time gave the same EPR detectable 7-line signal with a 2:4:3:4:3:4:2 hyperfine splitting pattern and coupling constants a_N =7.4 G, a_H = 3.6 G, and a_H = 3.9 G as shown in Fig. 4, panel a). DMPO (45 mM) or DNI (45 mM) alone irradiated in the same conditions gave no EPR signal, (Fig. S4).

In order to determine the DMPO adduct responsible of the EPR splitting pattern observed, we generated $^{\bullet}NO_2$ by an alternatively source of this radical, through UV photo-oxidation of an excess of $NaNO_2$ (300 mM in PBS pH 7.4) in presence of DMPO (45 mM) [50]. The hyperfine splitting pattern obtained reflects an acyclic DMPO-adduct derivative whether $^{\bullet}NO_2$ radical was generated by DNI photolysis or $NaNO_2$ under UV photo-oxidation, Fig. 4, panel a) [50]. After irradiation for 10 min the EPR cell containing DMPO and DNI mixture, the light was turned off and the EPR spectra were recorded for several minutes (1.5, 3, 4.5 min light-off). A time-dependent exponential decay was observed of EPR signal, showing a clear dependence on light irradiation, (Fig. 4, panel b).

Furthermore, simulations of EPR spectra based on previous reports of DMPO-NO_2 adduct acyclic derivative are in agreement with the experimentally observed, Fig. S5 [50]. Considering that nitrite is a by-product of DNI decomposition (due to one-electron reduction of $^{\bullet}NO_2$), we evaluated the potential contribution of NO_2^{-} upon UV-induced photo--oxidation to the $^{\bullet}NO_2$- dependent EPR signal observed. Assuming the complete decomposition of a 45 mM DNI solution, a theorical maximum equimolar concentration of nitrite could be produced. Therefore, we evaluated $^{\bullet}NO_2$-DMPO adduct formation at the same concentration of DNI used in Fig. 4. A very low EPR signal was obtained when DMPO (45 mM) was exposed to light for 5 min with an equal amount of $NaNO_2$ (45 mM), shown in Fig. S4 panel c), due to the requirement for a substantial nitrite concentration to initiate the formation of the $^{\bullet}NO_2$ radical *via* UV photo-oxidation.

Previous reports showed EPR detectable signal of nitro-anion radicals derived from the reduction of several nitroimidazoles used as drugs on anaerobic protozoal infections, even in absence of spin-trap DMPO in

[2] Note that $ABTS^{\bullet-}$ is also named as $ABTS^{\bullet+}$. [48] Re, R. et al., *Antioxidant activity applying an improved ABTS radical cation decolorization assay*. Free radical biology and medicine, 1999. **26**(9–10): p. 1231–1237.

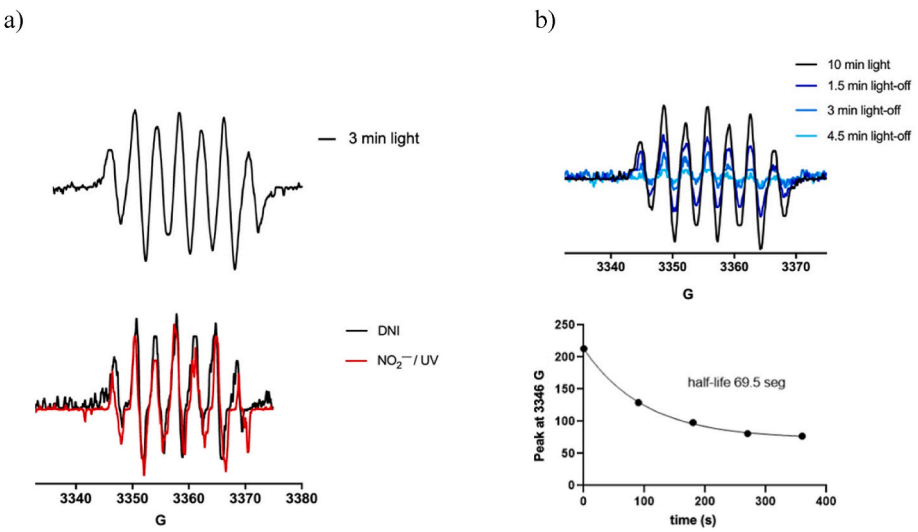

Fig. 4. EPR-spin trapping detection of $^{\bullet}NO_2$. a) EPR spectra of DMPO (45 mM) and DNI (45 mM) mixture generated after 3 min UV photolysis a 7-line signal with a 2:4:3:4:3:4:2 hyperfine splitting pattern and coupling constants (G) a_N =7.4, a_H = 3.6, and a_H = 3.9 was observed. Lower panel: EPR spectra of DMPO (45 mM) and DNI (45 mM) mixture generated after 5 min UV photolysis (black line), and EPR spectra of DMPO (45 mM) and ($NaNO_2$ 300 mM) adduct irradiated for 5 min (red line). b) Upper panel: same as a) but irradiated for 10 min and recorded every 1.5 min after turning off the light. Lower panel: Exponential decay of EPR signal with after turning off the light.

anaerobic conditions [51]. No evidence of $NI^{\bullet}$ or DMPO-$NI^{\bullet}$ adduct was observed by EPR analysis under our experimental conditions, all experiments were carried out under normal atmospheric conditions (*i.e.* 1 atm and 21% O_2).

Moreover, DNI (45 mM) was irradiated by UV–Vis lamp for 5 min in presence of DMPO (45 mM) in H_2O and the solution immediately analyzed by MS/MS. Precursor ion spectra of *m/z* 114 (corresponding to $DMPO^+$ fragment ion) was analyzed in order to identify potential DMPO adducts. A peak corresponding to the DMPO-NI adduct (*m/z* 240.8) and a peak at *m/z* 158.8 corresponding to the DMPO-NO_2 adduct were observed, only in presence of light, (Fig. 5 and Table S3).

Finally, we studied if O_2 has any contribution on the reaction mechanism of tyrosine nitration. As shown in Fig. S6, O_2 does not exert any effect on nitration reaction. This result discards an oxygen-derivative radical intermediate in the reaction of DNI [51,52].

Overall, these experiments support an homolytic cleavage of the RN-NO_2 bond of the nitramine moiety yielding $^{\bullet}NO_2$ and nitroimidazole radical ($NI^{\bullet}$) in agreement with previous reports [26,28,30].

3.5. Protein tyrosine nitration induced by DNI

In order to evaluate post-translational protein modifications generated by DNI photolysis, we studied DNI-induced protein tyrosine nitration in α-synuclein (α-syn), a key player in Parkinson's disease, among other synucleinopathies, development mechanism [53,54]. α-Synuclein is one of the main components of Lewy bodies and Lewy neurites found in synucleinopathies, and α-syn tyrosine nitration was reported within these anatomopathological hallmarks [8,55].

As we showed before, a fast nitration of free tyrosine was observed when samples were irradiated at 290 nm (Fig. 3), therefore α-syn was exposed to an irradiation for 10 and 30 min under 290 nm monochromatic light in the presence of DNI.

The formation of 3-nitrotyrosine was evidenced by western blot where an anti-3-nitrotyrosine monoclonal antibody signal was observed (Fig. 6 panel a) and mass spectrometry analysis confirmed these results (Fig. 6 panel b).

Nitrated α-syn dimers are also detected by western blot, probably due to di-tyrosine formation. This agrees with the formation of a tyrosyl radical intermediate upon the action of DNI, so part of this tyrosyl radical of one α-syn monomer reacts with another monomer tyrosyl radical and forms the di-tyrosine crosslink. This di-tyrosine formation in α-syn has been shown in α-syn treated with peroxynitrite [7], and it is appreciated in the positive control of nitrated α-syn (Fig. 6 line 4).

The addition of a nitro group (-NO_2) to a tyrosine residue results in an increase of +45 Da to the protein mass. Fig. 6 shows that in our experimental conditions, we were able to produce and detect nitration of

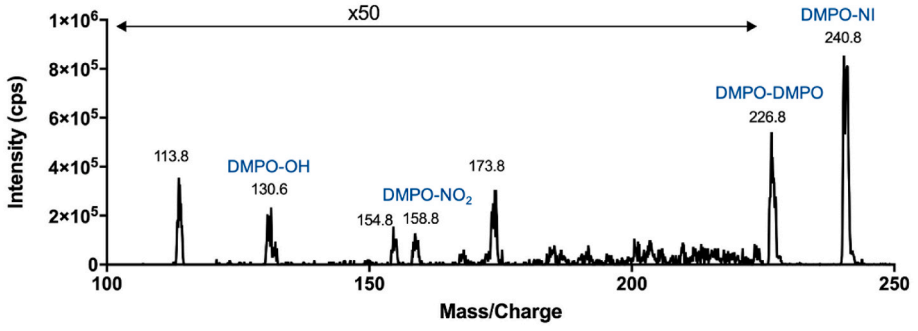

Fig. 5. MS of DMPO adducts upon DNI photolysis. Precursor Ion mass spectrum of DMPO (*m/z* = 113.8) after 5 min irradiation by UV–Vis lamp of a solution containing DNI (45 μM) and DMPO (45 μM) in H_2O. 50× represents the factor of amplification of the signal applied to the *m/z* range limited by the arrows.

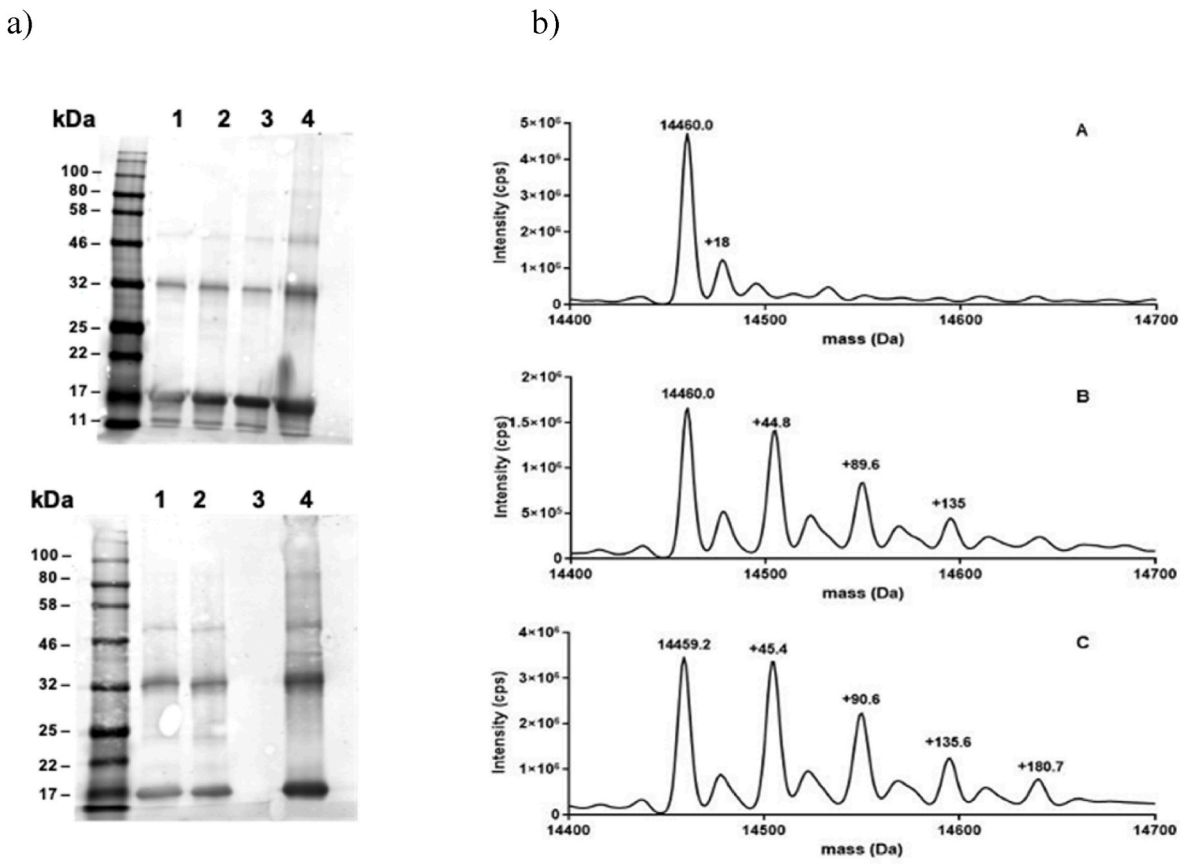

Fig. 6. DNI mediated α-syn nitration after irradiation at 290 nm. a) Western blot analysis of α-Syn (50 μM) mixed with DNI (500 μM) in 50 mM potassium phosphate buffer pH 6.0 and irradiated at 290 nm. Upper panel shows anti- α-syn; Lower panel shows anti 3-nitroTyr. Samples: 1) α-syn + DNI exposed for 10 min; 2) α-syn + DNI exposed for 30 min; 3) α-syn without DNI exposed for 30 min; 4) α-syn + $ONOO^-$ (1 mM). b) Mass spectrometry analysis of α-syn treated with DNI and monochromatic light irradiation at 290 nm. Mass spectra of (A) α-syn irradiated 30 min without DNI, (B) 10 min and (C) 30 min irradiation at 290 nm in the presence of DNI.

α-syn at a single (*ca.* 14459.2 Da +45 Da) and multiple tyrosine residues (*ca.* 14459.2 Da + [45]n.). A 10 min exposure, shows a change of +44.8 and +89.6 Da, corresponding with one nitro group, and two nitro groups incorporated in α-syn, respectively (Fig. 6 panel b). When the exposure time increases to 30 min, an increment in all nitrated species of α-syn was observed.(Fig. 6 panel b). Also, it is interesting to look at methionine oxidation in α-syn (Fig. 6) by DNI. α-Syn has four methionine residues per monomer, and during the purification a small amount of methionine sulfoxide is present (+18 Da). During the irradiation of α-syn in the presence of DNI, there is no significant increase of these +18 Da peaks (Fig. 6).

An exposure of α-syn to a 390 nm monochromatic light source in the presence of DNI, resulted in the formation of 3-nitrotyrosine, although higher irradiation time was required (30 min), as evidenced by western blot (Fig. S7 panel a) and mass spectrometry analysis (Fig. S7 panels b and c).

In order to test the efficiency of DNI-mediated tyrosine nitration of α-syn under the exposure to other light sources, we repeated these experiments irradiating the samples with a UVA tube (315–400 nm) and a UV–Vis 300 W lamp. In Fig. 7, we show the results of western blot analysis of α-syn (50 μM) with DNI (500 μM) for 30 min irradiation in 50 mM potassium phosphate buffer pH 6.0.

Mass spectrometry analysis of these samples showed a complete tyrosine nitration of α-syn when the reaction mixture was irradiated for 30 min with UVA (Fig. 7). With UV–Vis 300 W lamp irradiation, we detected the tri- and tetra-nitrated α-syn species, but also the tetra-nitrated α-syn with a single oxidized methionine residue (Fig. 7). These results show the importance of the light source on the efficiency of tyrosine nitration products. In the case of UV–Vis 300 W lamp, it generates a high energy light with an important heat effect, which depending of the exposure time, could evaporate and concentrate the protein solution. For the fluorimeter lamp, although it generates a monochromatic light, the intensity it is not enough to induce a complete nitration in α-syn at least during a 30 min incubation time (Fig. 6).

Being a $^{\bullet}NO_2$ donor, DNI also can also promote the one-electron oxidation of free- and protein-thiol groups [46,47]. This reactivity was demonstrated previously [26], by showing the conversion of a cysteine-containing peptide into cystine-dipeptide (disulfide bond) by DNI. Consequently, in proteins containing cysteine residues (not the case of α-syn), this competing oxidation process becomes a critical consideration.

3.6. *Intracellular $^{\bullet}NO_2$ production by DNI photolysis and cellular protein nitration*

In order to evaluate the possibility of using DNI as a nitrating agent in cellular cultures, its toxicity was first analyzed. Bovine aortic endothelial cells (BAECs) were incubated with different concentrations of DNI (0 μM–500 μM), with or without UVA light exposure for 10 min, then, cells were washed with dPBS and cultured for 24h in culture media. After that, cell viability was determined by MTT assay [38], (Fig. S8). Our results show that, cells that were incubated with DNI (0–250 μM)

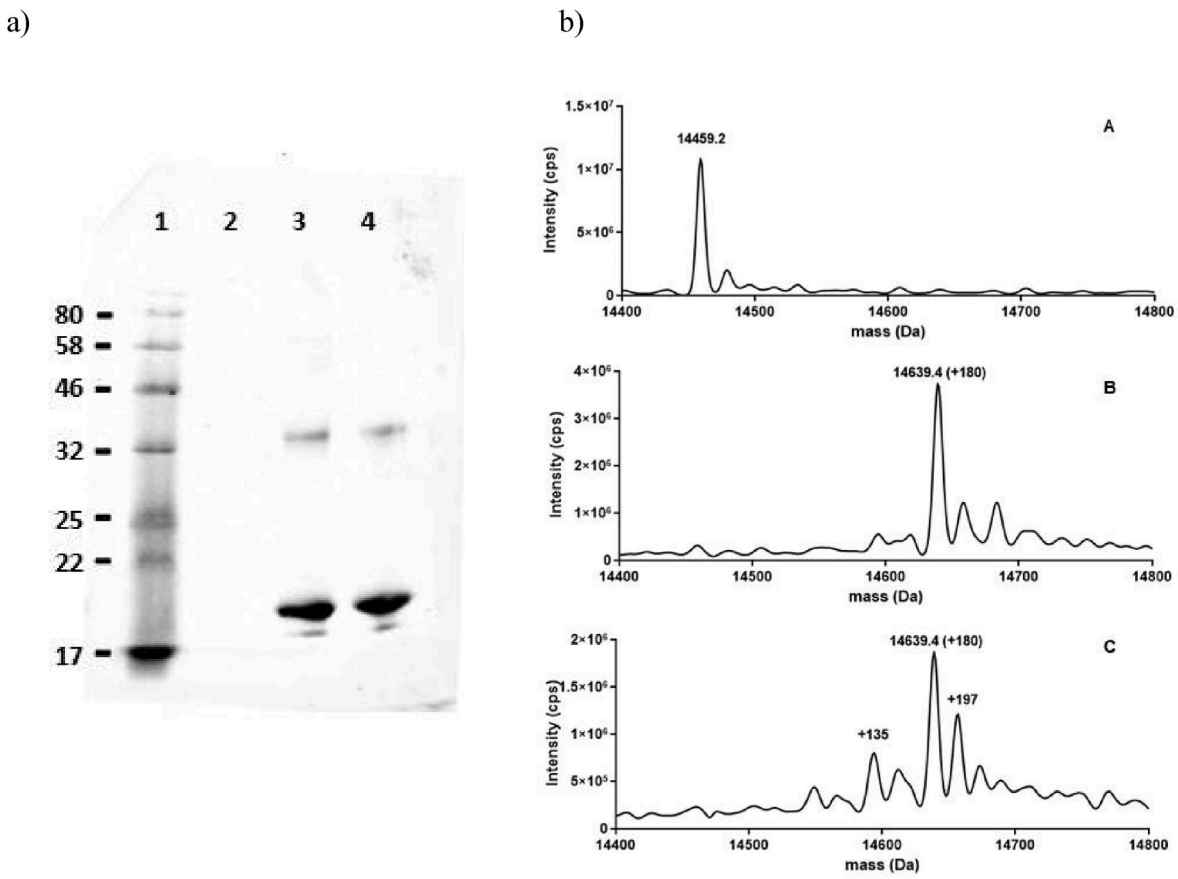

Fig. 7. DNI mediated α-syn nitration after UVA or UV–Vis irradiation. a) Western blot analysis of α-Syn (50 μM) mixed with DNI (500 μM) in 50 mM potassium phosphate buffer pH 6.0 and then irradiated for 30 min. Samples: 1) molecular weight marker; 2) α-syn (not irradiated and without DNI); 3) exposure to UVA light; 4) exposure to UV–Vis 300 W lamp.
b). Mass spectrometry analysis of DNI mediated α-syn nitration after irradiation with UVA and UV–Vis 300 W lamps. A) α-syn (not irradiated and without DNI); B) irradiated for 30 min with UVA; C) irradiated for 30 min with UV–Vis 300 W.

without light exposure had high viability (>80%), whereas those irradiated with UVA light (10 min) decreased the number of viable cells, probably due to the effect of $^{\bullet}NO_2$ fluxes. Higher concentrations of DNI (250–500 μM) decreased cell viability considerably *(i.e.* cell viability <30%), not shown), probably related to DNI toxicity. However, the incubation of BAECs with DNI (100 μM) exposed to 290 nm for 60 min, prior to cell incubation, was not toxic to cells (99% viability), indicating no toxicity of sub-product NI. In addition, the exposure to UVA light, without DNI, for 10 min also did not modify cell viability. Therefore, the incubation of cell cultures with 100–250 μM DNI and UVA light (10 min) allows the formation of intracellular $^{\bullet}NO_2$ fluxes with moderate cellular toxicity, Fig. S8.

DNI-mediated intracellular nitration in BAECs was confirmed by the use of the tyrosine analogue probe PHPA and detection and quantification of its nitrated product NO_2-HPA (Fig. 8, panel a). In this sense, BAECs pre-incubated with PHPA (1 mM), were treated with DNI (250 μM) and exposed to UVA light for 10 min. Under control conditions, a cell intake of *ca.* 4.2 nmol PHPA per well can be estimated Fig. S9. Then, the cellular content was extracted and NO_2-HPA was detected and quantified by HPLC-MS, Fig. 8, panel a). The estimation of intracellular

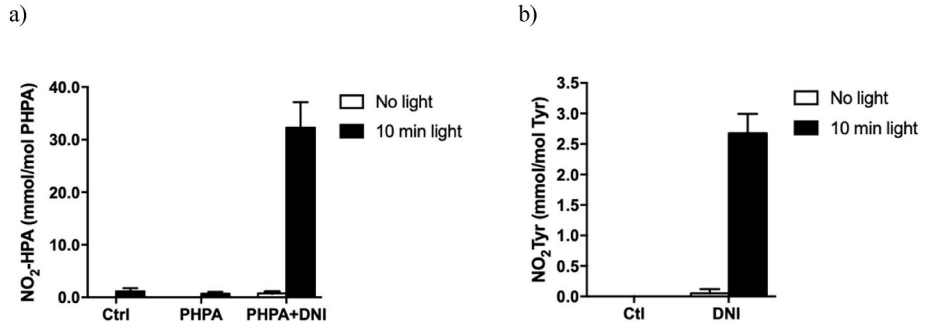

Fig. 8. Intracellular NO_2-HPA and protein nitration by DNI in BAECs. a) Ctrl: BAECs alone; PHPA: BAECs pre-incubated with PHPA (1 mM); PHPA + DNI: BAECs pre-incubated with PHPA (1 mM) and treated with DNI (250 μM), with or without UVA light. b) BAECs exposed to DNI (250 μM) was treated as in a) and protein 3-nitrotyrosine formation was estimated after acid-hydrolysis.

NO_2-HPA formation by DNI, upon UVA irradiation, was calculated as a ratio of total intracellular PHPA incorporated in control cells (*i.e.* absence of DNI).

Under similar conditions, intracellular protein 3-nitrotyrosine formation was measured in BAECs exposed to DNI using mass spectrometry and determining the 3-nitrotyrosine/tyrosine ratio after acid-hydrolysis (Fig. 8 panel b).

The results clearly show that DNI irradiated with UVA light was able to promote the nitration of both PHPA and protein tyrosine residues in BAECs. In the case of NO_2-PHPA a 30 mmol/mol PHPA ratio was quantified, meanwhile a *ca.* 3 mmol NO_2-Tyr/mol Tyr was measured. Whereas DNI alone did not cause nitration (Fig. 8).

In a cellular environment, $^{\bullet}NO_2$ has several competing targets in addition to tyrosine residues, including reduced glutathione, protein thiols and unsaturated lipids among others [56–58]. Thus, it is fully consistent that the extent of nitration observed for PHPA and protein tyrosine nitration formation (Fig. 8) is considerably lower in cellular settings compared to the *in vitro* experiment conducted with free PHPA or α-syn.

4. Conclusions

In this work, we describe a method for the synthesis of the photochemical nitrating agent DNI, and provide an extensive biochemical characterization and its applicability *in vitro* and *in cellula*. Our evidence further supports and expands previous work [26] on the production of $^{\bullet}NO_2$ upon light irradiation of DNI by inducing homolysis of N–NO_2 bond. NI$^{\bullet}$ radical is also produced during homolysis, and the effects of this species require additional investigation. The light source can modulate nitration reaction yields and kinetics. DNI can be utilized as a useful tool to generate nitrooxidative events in isolated proteins and cellular models. In summary, UVA-Vis light-triggered DNI homolysis provides the possibility to adjust $^{\bullet}NO_2$ fluxes to test different issues relevant for redox biochemistry and medicine, including $^{\bullet}NO_2$- and nitrotyrosine-dependent redox signaling mechanisms, oxidative damage and related redox-based pharmacological applications.

Declaration of competing interest

The authors declared no conflict or competing interest.

Acknowledgements

We thank Dr. Madia Trujillo and Dr. Anibal M. Reyes (Departamento de Bioquímica, Facultad de Medicina, Universidad de la República) for their valuable contribution on EPR discussions and assistance in MS experiments, respectively. MSc. Nelson Bracesco from Departamento de Biofísica, Facultad de Medicina, Universidad de la República for providing the different light sources used. Horacio Pezaroglio from Facultad de Química, Universidad de la República for performing RMN analysis. This work was supported by the Agencia Nacional de Investigación e Innovación (ANII) Uruguay (FCE_1_2019_156706) to JMS, Comisión Sectorial de Investigación Científica (CSIC) Grupos 2018 and Espacio Interdisciplinario 2020, Universidad de la República to RR. Fellowships from ANII and CSIC were awarded to RI. CC, NR, MM and AA are partially supported by FCE_1_2019_156706 and by Programa de Alimentos y Salud Humana (PAyS) IDB - R.O.U. (4950/OC-UR). Additional funding was obtained from Programa de Desarrollo de Ciencias Básicas (PEDECIBA, Uruguay).

Appendix A. Supplementary data

Supplementary data to this article can be found online at https://doi.org/10.1016/j.freeradbiomed.2023.09.038.

References

[1] R. Radi, Nitric oxide, oxidants, and protein tyrosine nitration, Proc. Natl. Acad. Sci. USA 101 (12) (2004) 4003–4008.
[2] P. Pacher, J.S. Beckman, L. Liaudet, Nitric oxide and peroxynitrite in health and disease, Physiol. Rev. 87 (1) (2007) 315–424.
[3] J.M. Souza, G. Peluffo, R. Radi, Protein tyrosine nitration—functional alteration or just a biomarker? Free Radical Biol. Med. 45 (4) (2008) 357–366.
[4] P. Wigner, et al., Oxidative stress parameters as biomarkers of bladder cancer development and progression, Sci. Rep. 11 (1) (2021), 15134.
[5] E. Fernández-Espejo, et al., Native α-synuclein, 3-nitrotyrosine proteins, and patterns of nitro-α-synuclein-immunoreactive inclusions in saliva and submandibulary gland in Parkinson's disease, Antioxidants 10 (5) (2021) 715.
[6] M. Bandookwala, P. Sengupta, 3-Nitrotyrosine: a versatile oxidative stress biomarker for major neurodegenerative diseases, Int. J. Neurosci. 130 (10) (2020) 1047–1062.
[7] J.M. Souza, et al., Dityrosine cross-linking promotes formation of stable α-synuclein polymers: implication of nitrative and oxidative stress in the pathogenesis of neurodegenerative synucleinopathies, J. Biol. Chem. 275 (24) (2000) 18344–18349.
[8] B.I. Giasson, et al., Oxidative damage linked to neurodegeneration by selective α-synuclein nitration in synucleinopathy lesions, Science 290 (5493) (2000) 985–989.
[9] A. Baillet, et al., The role of oxidative stress in amyotrophic lateral sclerosis and Parkinson's disease, Neurochem. Res. 35 (10) (2010) 1530–1537.
[10] L. Thomson, 3-nitrotyrosine Modified Proteins in Atherosclerosis, vol. 2015, Disease markers, 2015.
[11] G. Peluffo, R. Radi, Biochemistry of protein tyrosine nitration in cardiovascular pathology, Cardiovasc. Res. 75 (2) (2007) 291–302.
[12] H. Kaur, B. Halliwell, Evidence for nitric oxide-mediated oxidative damage in chronic inflammation Nitrotyrosine in serum and synovial fluid from rheumatoid patients, FEBS Lett. 350 (1) (1994) 9–12.
[13] H. Ahsan, 3-Nitrotyrosine, A biomarker of nitrogen free radical species modified proteins in systemic autoimmunogenic conditions, Hum. Immunol. 74 (10) (2013) 1392–1399.
[14] M. Kedzierska, et al., The nitrative and oxidative stress in blood platelets isolated from breast cancer patients: the protectory action of aronia melanocarpa extract, Platelets 21 (7) (2010) 541–548.
[15] R. Radi, et al., Unraveling peroxynitrite formation in biological systems, Free Radic. Biol. Med. 30 (5) (2001) 463–488.
[16] S. Bartesaghi, R. Radi, Fundamentals on the biochemistry of peroxynitrite and protein tyrosine nitration, Redox Biol. 14 (2018) 618–625.
[17] R. Radi, Protein tyrosine nitration: biochemical mechanisms and structural basis of functional effects, Acc. Chem. Res. 46 (2) (2013) 550–559.
[18] C.X. Santos, M.G. Bonini, O. Augusto, Role of the carbonate radical anion in tyrosine nitration and hydroxylation by peroxynitrite, Arch. Biochem. Biophys. 377 (1) (2000) 146–152.
[19] S. Goldstein, et al., Tyrosine nitration by simultaneous generation of· NO and O-· 2 under physiological conditions HOW the radicals DO the job, J. Biol. Chem. 275 (5) (2000) 3031–3036.
[20] T.C. Bruice, M.J. Gregory, S.L. Walters, Reactions of tetranitromethane. I. Kinetics and mechanism of nitration of phenols by tetranitromethane, J. Am. Chem. Soc. 90 (6) (1968) 1612–1619.
[21] M. Sokolovsky, D. Harell, J.F. Riordan, Reaction of tetranitromethane with sulfhydryl groups in proteins, Biochemistry 8 (12) (1969) 4740–4745.
[22] B.S. Rocha, et al., Pepsin is nitrated in the rat stomach, acquiring antiulcerogenic activity: a novel interaction between dietary nitrate and gut proteins, Free Radical Biol. Med. 58 (2013) 26–34.
[23] G.A. Olah, S.C. Narang, J.A. Olah, Nitration of naphthalene and remarks on the mechanism of electrophilic aromatic nitration, Proc. Natl. Acad. Sci. USA 78 (6) (1981) 3298–3300.
[24] H. Jiang, M. Balazy, Detection of 3-nitrotyrosine in human platelets exposed to peroxynitrite by a new gas chromatography/mass spectrometry assay, Nitric Oxide 2 (5) (1998) 350–359.
[25] M. Ponczek, P. Nowak, B. Wachowicz, The effects of nitronium ion on nitration, carbonylation and coagulation of human fibrinogen, Gen. Physiol. Biophys. 27 (1) (2008) 55.
[26] T. Long, et al., Light-controlled tyrosine nitration of proteins, Angew. Chem. Int. Ed. 60 (24) (2021) 13414–13422.
[27] B. Duan, et al., Screening for energetic compounds based on 1, 3-dinitrohexahydropyrimidine skeleton and 5-various explosopheres: molecular design and computational study, Sci. Rep. 10 (1) (2020) 1–13.
[28] M. Pace, B. Holmes, Spin trapping of. NO2 radicals produced by uv photolysis of RDX, HMX, and nitroguanidine, J. Magn. Reson. 52 (1) (1983) 143–146.
[29] M. Pace, Spin trapping of nitrogen dioxide from photolysis of sodium nitrite, ammonium nitrate, ammonium dinitramide, and cyclic nitramines, J. Phys. Chem. 98 (25) (1994) 6251–6257.
[30] M. Pace, B. Kalyanaraman, Spin trapping of nitrogen dioxide radical from photolytic decomposition of nitramines, Free Radical Biol. Med. 15 (3) (1993) 337–342.
[31] R. Radi, et al., Peroxynitrite oxidation of sulfhydryls. The cytotoxic potential of superoxide and nitric oxide, J. Biol. Chem. 266 (7) (1991) 4244–4250.
[32] M.R. Grimmett, et al., 1, 4-Dinitroimidazole and derivatives. Structure and thermal rearrangement, J Australian Journal of Chemistry 42 (8) (1989) 1281–1289.
[33] D.A. Malencik, et al., Dityrosine: preparation, isolation, and analysis, Anal. Biochem. 242 (2) (1996) 202–213.

[34] M. Wrona, K. Patel, P. Wardman, Reactivity of 2′, 7′-dichlorodihydrofluorescein and dihydrorhodamine 123 and their oxidized forms toward carbonate, nitrogen dioxide, and hydroxyl radicals, Free Radic. Biol. Med. 38 (2) (2005) 262–270.
[35] V. Chechik, D. Murphy, E. Carter. https://www.eprsimulator.org/isotropic.html, 2020.
[36] P.H. Weinreb, et al., NACP, a protein implicated in Alzheimer's disease and learning, is natively unfolded, Biochemistry 35 (43) (1996) 13709–13715.
[37] C. Brito, et al., Peroxynitrite inhibits T lymphocyte activation and proliferation by promoting impairment of tyrosine phosphorylation and peroxynitrite-driven apoptotic death, J. Immunol. 162 (6) (1999) 3356–3366.
[38] M.V. Berridge, A.S. Tan, Characterization of the cellular reduction of 3-(4, 5-dimethylthiazol-2-yl)-2, 5-diphenyltetrazolium bromide (MTT): subcellular localization, substrate dependence, and involvement of mitochondrial electron transport in MTT reduction, J Archives of Biochemistry Biophysics 303 (2) (1993) 474–482.
[39] L.F. Gamon, et al., Absolute quantitative analysis of intact and oxidized amino acids by LC-MS without prior derivatization, Redox Biol. 36 (2020), 101586.
[40] S.J. Nicholls, et al., Quantification of 3-nitrotyrosine levels using a benchtop ion trap mass spectrometry method, Methods Enzymol. 396 (2005) 245–266.
[41] A.D. McNaught, A. Wilkinson, Compendium of Chemical Terminology, IUPAC Recommendations, Vol 1669, Blackwell Science, Oxford, 1997.
[42] R.N. Jones, G.D. Thorn, The ultraviolet absorption spectra of aliphatic nitramines, nitrosamines, and nitrates, J Canadian Journal of Research 27 (11) (1949) 828–860.
[43] J.S. Beckman, et al., Kinetics of superoxide dismutase-and iron-catalyzed nitration of phenolics by peroxynitrite, Arch. Biochem. Biophys. 298 (2) (1992) 438–445.
[44] N. Campolo, Thesis: Nitración y oxidación de tirosina por peroxinitrito mediada por metales de transición, in: Departamento de Bioquímica, Universidad de la República, 2013. https://www.colibri.udelar.edu.uy/jspui/handle/20.500.12008/1525.
[45] S. Bartesaghi, et al., Lipid peroxyl radicals mediate tyrosine dimerization and nitration in membranes, Chem. Res. Toxicol. 23 (4) (2010) 821–835.
[46] W.A. Prütz, et al., Reactions of nitrogen dioxide in aqueous model systems: oxidation of tyrosine units in peptides and proteins, Arch. Biochem. Biophys. 243 (1) (1985) 125–134.
[47] E. Ford, M.N. Hughes, P. Wardman, Kinetics of the reactions of nitrogen dioxide with glutathione, cysteine, and uric acid at physiological pH, Free Radic. Biol. Med. 32 (12) (2002) 1314–1323.
[48] R. Re, et al., Antioxidant activity applying an improved ABTS radical cation decolorization assay, Free Radic. Biol. Med. 26 (9–10) (1999) 1231–1237.
[49] M.N. Möller, et al., Detection and quantification of nitric oxide–derived oxidants in biological systems, J. Biol. Chem. 294 (40) (2019) 14776–14802.
[50] K.M. Nash, A. Rockenbauer, F.A. Villamena, Reactive nitrogen species reactivities with nitrones: theoretical and experimental studies, Chem. Res. Toxicol. 25 (8) (2012) 1581–1597.
[51] N. Yarlett, et al., Nitroimidazole and oxygen derived radicals detected by electron spin resonance in hydrogenosomal and cytosolic fractions from Trichomonas vaginalis, Mol. Biochem. Parasitol. 24 (3) (1987) 255–261.
[52] L.K. Folkes, et al., Radiolysis studies of oxidation and nitration of tyrosine and some other biological targets by peroxynitrite-derived radicals, Int. J. Mol. Sci. 23 (3) (2022) 1797.
[53] L.V. Kalia, A.E. Lang, Parkinson's disease, Lancet 386 (9996) (2015) 896–912.
[54] M. Goedert, R. Jakes, M.G. Spillantini, The synucleinopathies: twenty years on, J. Parkinsons Dis. 7 (s1) (2017) S51–S69.
[55] C. Chavarría, J.M. Souza, Oxidation and nitration of α-synuclein and their implications in neurodegenerative diseases, Arch. Biochem. Biophys. 533 (1–2) (2013) 25–32.
[56] M. Trujillo, et al., Peroxynitrite-derived carbonate and nitrogen dioxide radicals readily react with lipoic and dihydrolipoic acid, Free Radic. Biol. Med. 39 (2) (2005) 279–288.
[57] B. Halliwell, et al., Interaction of nitrogen dioxide with human plasma Antioxidant depletion and oxidative damage, FEBS Lett. 313 (1) (1992) 62–66.
[58] D.B. Hood, P. Gettins, D.A. Johnson, Nitrogen dioxide reactivity with proteins: effects on activity and immunoreactivity with α-1-proteinase inhibitor and implications for NO2-mediated peptide degradation, Arch. Biochem. Biophys. 304 (1) (1993) 17–26.